Molecular Mechanisms and Binding Site Location for the Noncompetitive Antagonist Crystal Violet on Nicotinic Acetylcholine Receptors†

Hugo R. Arias,*,§ Pankaj Bhumireddy,§ Guillermo Spitzmaul,‡ James R. Trudell,|| and Cecilia Bouzat‡

Department of Pharmaceutical Sciences, College of Pharmacy, Western University of Health Sciences, Pomona, California 91766-1854, Instituto de Investigaciones Bioquímicas de Bahía Blanca, Universidad Nacional del Sur-CONICET, Camino La Carrindanga Km 7, B8000FWB, Bahía Blanca, Argentina, and Department of Anesthesia, Stanford University School of Medicine, Stanford, California 94305-5117

Received August 30, 2005; Revised Manuscript Received December 22, 2005

ABSTRACT: We investigated the molecular mechanisms and the binding site location for the fluorophor crystal violet (CrV), a noncompetitive antagonist of the nicotinic acetylcholine receptor (AChR). To this end, radiolabeled competition binding, fluorescence spectroscopy, Schild-type analysis, patch-clamp recordings, and molecular dynamics approaches were used. The results indicate that (i) CrV interacts with the desensitized *Torpedo* AChR with higher affinity than with the resting state at several temperatures (5−37 °C); (ii) CrV-induced inhibition of the phencyclidine (PCP) analogue [^{3}H]thienylcyclohexylpiperidine binding to the desensitized or resting AChR is mediated by a steric mechanism; (iii) tetracaine inhibits CrV binding to the resting AChR, probably by a steric mechanism; (iv) barbiturates modulate CrV binding to the resting AChR by an allosteric mechanism; (v) CrV itself induces AChR desensitization; (vi) CrV decreases the peak of macroscopic currents by acting on the resting AChR but without affecting the desensitization rate from the open state; and (vii) two tertiary amino groups from CrV may bind to the α1-Glu^{262} residues (located at position 20′) in the resting state. We conclude that the CrV binding site overlaps the PCP locus in the resting and desensitized state. The noncompetitive action of CrV may be explained by an allosteric mechanism in which the binding of CrV to the extracellular mouth of the resting receptor leads to an inhibition of channel opening. Binding of CrV probably increases desensitization of the resting channel and stabilizes the desensitized state.

The nicotinic acetylcholine receptor (AChR)[1] is the archetype of the Cys-loop ligand-gated ion channel superfamily found in the nervous system. This receptor superfamily includes types A and C γ-aminobutyric acid, type 3 5-hydroxytryptamine (serotonin), and glycine receptors (reviewed in refs *1*−*4*). This superfamily is important in mediating synaptic transmission in the nervous system and contributes to higher order brain mechanisms such as memory, learning, perception, cognition, and emotion (reviewed in refs *3* and *5*). The malfunctioning of these receptors has been considered as the origin of several neuropsychiatric disorders (reviewed in refs *3* and *5*).

Agonist-induced activation of AChRs can be inhibited by compounds referred to as noncompetitive antagonists (NCAs). NCAs represent a structurally diverse group of compounds that include exogenous (e.g., local and general anesthetics, among others) as well as endogenous molecules (e.g., neurosteroids, substance P, among others) (reviewed in refs *6*−*8*). The noncompetitive inhibition of the receptor function likely occurs via several different mechanisms: (i) an open-channel blocking mechanism (some NCAs may inhibit the AChR by simply binding within the pore of the ion channel when the receptor is in the open state, thereby physically blocking ion permeation); (ii) several allosteric mechanisms: (a) NCAs may inhibit receptor function by preferentially binding to and stabilizing a nonconducting conformational state of the AChR (e.g., resting or desensitized states), and/or (b) these drugs may increase the AChR desensitization rate and decrease the probability of channel opening. These two latter mechanisms may be triggered by NCA binding to sites that are located apart from the ion

† This research was supported by Western University of Health Sciences Intramural Grants (H.R.A.), the Master in Sciences Program, Department of Pharmaceutical Sciences (P.B.), and by grants from CONICET, Universidad Nacional del Sur, Agencia Nacional de Promoción Científica y Tecnológica and a Guggenheim Fellowship (C.B.).

* To whom correspondence should be addressed: Department of Pharmaceutical Sciences, College of Pharmacy, Western University of Health Sciences, 309 E. Second St., Pomona, CA 91766-1854, USA. Telephone: (909) 469−5424. Fax: (909) 469−5600. E-mail: harias@westernu.edu.

§ Western University of Health Sciences.

‡ Instituto de Investigaciones Bioquímicas de Bahía Blanca (INIBIBB).

|| Stanford University School of Medicine.

[1] Abbreviations: AChR, nicotinic acetylcholine receptor; PCP, phencyclidine; [^{3}H]TCP, [piperidyl-3, 4−3H(*N*)]-(*N*-(1-(2 thienyl)-cyclohexyl)-3,4-piperidine); CCh, carbamylcholine; ACh, acetylcholine; α-BTx, α-bungarotoxin; CrV, crystal violet; RT, room temperature; BS buffer, binding saline buffer (50 mM Tris-HCl, 120 mM NaCl, 5 mM KCl, 2 mM $CaCl_2$, 1 mM $MgCl_2$, pH 7.4); NCA, noncompetitive antagonist; TID, 3-(3-iodophenyl)-3-(trifluoromethyl)-diazirine; DTMA (dansyltrimethylamine), [1-(dimethylamino)-naphthalene-5-sulfonamido]ethyltrimethylammonium perchlorate; K_i, inhibition constant; K_d, dissociation constant; IC_{50}, ligand concentration that produces 50% AChR binding or function inhibition; τ_d, decay time constant; n_H, Hill coefficient; r^2, goodness of fit; $EC_{50}^{R\rightarrow D}$, ligand concentration that produces 50% AChR desensitization; P_{open}, probability of channel opening.

10.1021/bi051752e CCC: $33.50
Published on Web 01/27/2006

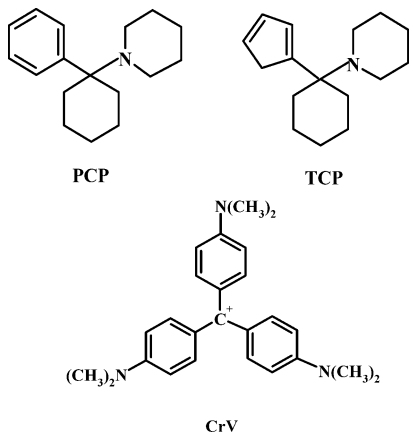

FIGURE 1: Molecular structure for the NCAs phencyclidine (PCP), its structural and functional analogue thienylcyclohexylpiperidine (TCP), and the fluorescent probe crystal violet (CrV).

channel proper, the so-called nonluminal binding sites (reviewed in ref *6*). Further, it is also likely that many NCAs inhibit receptor function by utilizing more than one mechanism.

From the results of equilibrium binding experiments it was observed that [^{3}H]thienylcyclohexylpiperidine ([^{3}H]TCP), a structural and functional analogue of the hallucinogen and general anesthetic phencyclidine (PCP) (see ref *9*), binds to a single high-affinity locus in the resting as well as in the desensitized AChR ion channel (*10*, *11*). Figure 1 shows the molecular structure of these two PCP analogues, as well as for the fluorophor and NCA crystal violet (CrV). Many attempts have been made to characterize the PCP locus using different approaches but without much success (reviewed in refs *6*−*8*). In this regard, the use of fluorophores to characterize the PCP locus by using fluorescence spectroscopy is an alternative approach. Previous fluorescence studies have shown that the NCA CrV binds to a PCP-sensitive locus within the AChR with high affinity (*12*). However, there is not clear-cut evidence for either the inhibitory mechanism elicited by CrV on the AChR or the structural characteristics of its binding site. Thus, we plan to characterize the CrV binding site as well as to determine its inhibitory mechanism on the AChR.

There are two objectives of this work. The first objective is to characterize the CrV binding site in the resting and desensitized state, and the second objective is to determine the noncompetitive inhibitory mechanisms for the fluorophore. Regarding our first objective, we studied the location of CrV binding site by competitive binding experiments between [^{3}H]TCP and CrV in the resting and desensitized state. To determine the mechanism of interaction of CrV with the PCP binding site, Schild plot analyses as well as thermodynamic experiments were carried out. To further characterize the CrV locus in the resting state, Schild plot analyses were performed using tetracaine and different barbiturates (e.g., amobarbital and pentobarbital). In addition, molecular modeling was performed to provide a graphical illustration of putative binding sites. For our second objective, we performed electrophysiological experiments using patch-clamp techniques. Finally, we determined that CrV desensitizes the AChR by studying the effect of CrV on the binding of the fluorescent agonist dansyltrimethylamine (DTMA).

The characterization of the CrV binding site will help to determine the structural and functional properties of the AChR ion channel in different conformational states as well as to determine the structure of the PCP locus. The characterization of the PCP locus is of significant importance because it is the target domain for a series of potentially relevant compounds that includes antidepressants (*13*), adamantane derivatives (*10*), and anabaseine analogues (*14*). These compounds could be used therapeutically for the treatment of depression, Parkinson's disease, and Alzheimer's disease, respectively.

EXPERIMENTAL PROCEDURES

Materials. [Piperidyl-3,4-^{3}H(*N*)]-(*N*-(1-(2-thienyl)cyclohexyl)-3,4-piperidine) ([^{3}H]TCP; 45.2 Ci/mmol) was obtained from PerkinElmer Life Sciences, Inc. (Boston, MA) and stored in ethanol at −20 °C. Carbamylcholine chloride (CCh), acetylcholine chloride (ACh), suberylcholine dichloride, proadifen hydrochloride, amobarbital hydrochloride, pentobarbital hydrochloride, phencyclidine hydrochloride (PCP), tetracaine hydrochloride, and polyethylenimine were purchased from Sigma Chemical Co. (St. Louis, MO). Crystal violet hydrochloride (CrV) was obtained from Aldrich Chemical Co., Inc. (Milwaukee, WI). [1-(Dimethylamino)naphthalene-5-sulfonamido]ethyltrimethylammonium perchlorate (dansyltrimethylamine; DTMA) was obtained from Pierce Chemical Co. (Rockford, IL). α-Bungarotoxin (α-BTx) was obtained from Molecular Probes (Eugene, OR). Salts were of analytical grade.

Preparation of AChR Native Membranes. AChR native membranes were prepared from frozen *Torpedo californica* electric organs (Aquatic Research Consultants, San Pedro, CA) by differential and sucrose density gradient centrifugation, as described previously (*15*). Total AChR membrane protein was determined using the BCA protein assay (Pierce Chemical Co.). Specific activities of these membrane preparations were determined by the decrease in DTMA (6.6 μM) fluorescence produced by the titration of suberyldicholine into receptor suspensions (0.3 mg/mL) in the presence of 100 μM PCP. The activities ranged from 0.9 to 1.2 nmol of suberyldicholine binding sites/mg of total protein (0.45−0.60 nmol of AChR/mg of protein). The AChR membrane preparations were stored at −80 °C in 12% sucrose.

Fluorescence Measurements. All fluorescence titrations were carried out in 3-mm quartz cuvettes using a Flurolog-3 spectroflourimeter (Horiba-Jobin-Yvon, Edison, NJ). Crystal violet excitation and emission wavelengths were 600 and 645 nm, respectively. To reduce stray-light effects, a 600-nm narrow band and a 630-nm cutoff filter were placed in the path of excitation and emission beams, respectively. Dansyltrimethylamine excitation and emission wavelengths were 295 and 546 nm, respectively. To reduce stray-light effects, a 530-nm cutoff filter was placed in the path of the emission wavelength.

Crystal Violet Binding Affinity in Different Conformational States of the AChR. To determine the binding affinity of CrV in the resting and desensitized state, direct titrations of CrV into AChR membranes (0.3 μM) were performed at room temperature (RT). The membranes were suspended in binding saline (BS) buffer (50 mM Tris-HCl, 120 mM NaCl, 5 mM KCl, 2 mM $CaCl_2$, 1 mM $MgCl_2$, pH 7.4), in the absence

(resting state) or in the presence of 1 mM carbamylcholine (CCh) (desensitized state). Nonspecific binding was obtained in the presence of 100 μM PCP. Estimates of the K_d values for CrV were made by fitting the plots of the PCP-sensitive changes in CrV fluorescence versus free CrV concentration to a four parameter logistic equation (sigmoid) by means of the Prism program (GraphPAD Software, San Diego, CA) using the following equation.

$$B = (B_{max}[L]^{n_H})/([L]^{n_H} + K_d^{n_H}) \quad (1)$$

where B is the specifically bound ligand, B_{max} is the maximum binding at equilibrium, [L] is the free ligand concentration, K_d is the equilibrium dissociation constant, and n_H is the Hill coefficient. Free CrV concentration was calculated using the Marquardt algorithm (*16*).

To study the thermodynamic parameters of CrV binding, the CrV K_d was determined at different temperatures (e.g., 5, 15, 25, and 37 °C) when the receptor is in either the resting or the desensitized state.

Crystal Violet-Induced [^{3}H]TCP Binding Inhibition. To determine the effect of CrV on [^{3}H]TCP maximal binding to the *Torpedo* AChR, AChR native membranes (0.3 μM) were suspended in BS buffer, with ~7 nM [^{3}H]TCP, in the presence of 1 mM CCh (desensitized) or 1 μM α-BTx (resting) and preincubated for 30 min at RT. α-Bungarotoxin is a competitive antagonist that maintains the AChR in the resting state (*17*). Nonspecific binding was determined in the presence of 100 μM PCP (desensitized) or 200 μM tetracaine (resting). The total volume was divided into aliquots, increasing concentrations of CrV (1 nM to 200 μM) were added to each tube, and the mixtures were incubated for 2 h at RT. AChR-bound [^{3}H]TCP was then separated from free ligand by a filtration assay using a 48-sample harvester system (Brandel Inc., Gaithersburg, MD) with GF/B Whatman filters (obtained from Brandel), previously soaked with 0.5% polyethylenimine for 30 min. The membrane-containing filters were transferred to scintillation vials containing 3 mL of Bio-Safe II (Research Product International Corp, Mount Prospect, IL), and the radioactivity was determined using a Beckman LS 6000IC scintillation counter (Beckman Coulter, Inc., Fullerton, CA). For the competition binding experiments described above, the concentration−response data were curve-fitted by nonlinear least-squares analysis using the Prism program (GraphPAD Software, San Diego, CA). The corresponding IC_{50} values were calculated using the following equation:

$$\theta = 1/[(1 + ([L]^{n_H}/IC_{50})] \quad (2)$$

where θ is the fractional amount of [^{3}H]TCP bound in the presence of inhibitor at a concentration [L] compared to the amount of [^{3}H]TCP bound in the absence of inhibitor (total binding). IC_{50} is the ligand concentration at which $\theta = 0.5$ (50% bound).

Taking into account that the AChR presents one binding site for TCP in the desensitized (*9*) or in the resting state (*10*), the observed IC_{50} values from the competition experiments were transformed into inhibition constant (K_i) values using the Cheng-Prusoff relationship (*18*):

$$K_i = IC_{50}/\{1 + ([TCP]/K_d^{TCP})\} \quad (3)$$

where [TCP] is the initial concentration of [^{3}H]TCP and K_d^{TCP} is the dissociation constant for [^{3}H]TCP [0.83 μM in the resting state (*10*) and 0.25 μM in the desensitized state (*9*)].

Schild Plot Analyses. To determine whether CrV inhibits [^{3}H]TCP binding to the AChR by a steric or an allosteric mechanism, CrV-induced inhibition of [^{3}H]TCP was measured at increasing initial concentrations of [^{3}H]TCP + unlabeled PCP (e.g., 3.1, 6.2, and 9.3 μM). We used unlabeled PCP instead of unlabeled TCP on these experiments because TCP is not commercially available and because [^{3}H]PCP has the same affinity (0.30 ± 0.10 μM) for the *Torpedo* AChR as that for [^{3}H]TCP (0.25 ± 0.04 μM) (*9*). The rationale of this experiment is that, for a higher initial concentration of an AChR-bound ligand, we will need a higher concentration of the competitor to produce a total ligand binding inhibition. This rationale is consistent with Schild-type analysis (*19*). From these competition curves, the apparent IC_{50} values were calculated. Then, we plotted the ratio between the IC_{50} values for CrV determined at different initial concentrations of PCP under the IC_{50} control values (no PCP added) versus the initial PCP concentration ($IC_{50}^{PCP}/IC_{50}^{control}$ versus $[PCP]_{initial}$) (for more details see ref *11*). A linear relationship from this modified Schild plot indicates a competitive interaction, whereas a nonlinear relationship suggests an allosteric mechanism of inhibition (*11*, *19*).

Schild Plot Analyses of Barbiturate- or Tetracaine-Induced Inhibition of Crystal Violet Binding to the Resting AChR. The apparent K_d for CrV in the presence of different concentrations of tetracaine or different barbiturates was measured. In this regard, AChR membranes were suspended in BS buffer and preincubated with different initial concentrations of tetracaine (e.g., 0.5, 0.7, 1, or 2 μM), amobarbital (e.g., 5, 10, or 20 μM), or pentobarbital (e.g., 0.2, 0.5, 0.8, or 1.5 mM), in the absence of CCh (resting). To obtain the nonspecific binding, 200 μM tetracaine or alternatively 100 μM PCP was used. To determine whether CrV inhibits tetracaine or amobarbital binding to the AChR by a steric or allosteric mechanism, Schild plot analyses were performed according to the equation (*19*):

$$\log[(K_d^{competitor}/K_d) - 1] = \log(pA_2) - \log K_i \quad (4)$$

where K_d and $K_d^{competitor}$ are the apparent dissociation constants of CrV in the absence or in the presence of a certain concentration of the competitor (e.g., tetracaine or amobarbital), and pA_2 is the negative logarithm of the competitor concentration that reduces the apparent affinity of CrV by a factor of 2 (for more details see ref *20*). When $K_d^{competitor} = K_d$ then, $\log[(K_d^{competitor}/K_d) - 1] = 0$, and $\log(pA_2) = -\log K_i$. In this regard, the K_i value can be graphically calculated as the antilog of the *x*-intercept (when $y = 0$) from the $\log[(K_d^{competitor}/K_d) - 1]$ versus log[competitor] plot. To determine whether a steric or an allosteric mechanism elicits the observed displacement, the slope of the Schild plot was also considered. A slope of one or near unity is indicative of a steric mechanism, whereas a slope value far from unity (e.g., <0.5 or >2) suggests an allosteric-type of inhibition (*19*, *20*).

Since pentobarbital preincubation increased PCP-sensitive CrV fluorescence in the resting but activatable state (no

α-BTx), we wanted to determine the mechanism underlying this CrV binding enhancement. In this regard, AChR membranes (0.3 μM) were preincubated with 1.5 mM pentobarbital in the absence (resting but activatable) or in the presence of 1 μM α-BTx (resting).

Crystal Violet-Induced AChR Desensitization. To determine whether CrV induces receptor desensitization, AChR native membranes were suspended in BS buffer in the presence of the fluorescent agonist DTMA (~6 μM) and incubated for 10 min at RT in the resting but activatable state (no ligands). Then, CrV was titrated and the DTMA fluorescence was monitored as explained in the previous section (see Fluorescence Measurements). The nonspecific binding was determined in the presence of 1 mM CCh. Additionally, CrV titration in the resting state was compared with that for proadifen. Proadifen is a local anesthetic that desensitizes the AChR (*21*). A control experiment was also carried out between CrV and DTMA specific fluorescence in the desensitized AChR. To this end, AChR membranes were preincubated with 200 μM proadifen. We expected that CrV would not increase DTMA fluorescence when the AChR was already in the desensitized state. Corrections for CrV absorption at excitation and emission wavelengths of DTMA were performed according to the equation (*22*):

$$F_{cor} = F_{app}/\{10^{-Aex\ (Lex/2)[C]/[Cex]} \times 10^{-Aem(Lem/2)[C]/[Cem]}\} \quad (5)$$

where F_{corr} and F_{app} are the corrected and apparent fluorescence intensities of DTMA, [C] is the concentrations of CrV used in the fluorescence experiments, $[C_{ex}]$ and $[C_{em}]$ are the CrV concentrations used to determine absorption at the excitation (A_{ex}) and emission (A_{em}) wavelengths, respectively, and L_{ex} and L_{em}, are the path lengths of the cuvette along the excitation and emission axes, respectively.

Cell Expression of Mouse Muscle AChR. HEK293 (Human embryonic kidney) cells were transfected with mouse α, β, δ, and ϵ cDNA subunits using calcium phosphate precipitation at a subunit ratio of 2:1:1:1 for α:β:δ:ϵ, respectively, essentially as previously described (*23*). Cells were used for single-channel measurements 1 or 2 days after transfection.

Patch-Clamp Recordings. Macroscopic currents were recorded in the outside-out patch configuration (*24*). The pipet solution contained 140 mM KCl, 5 mM EGTA, 5 mM $MgCl_2$, and 10 mM HEPES, pH 7.3. Extracellular solution contained 150 mM NaCl, 5.6 mM KCl, 1.8 mM $CaCl_2$, 5 mM $MgCl_2$, and 10 mM HEPES, pH 7.3. The patch was excised in this configuration and moved into position at the outflow of a perfusion system (*25*, *26*). The perfusion system allows for a rapid (0.1−1 ms) exchange of the solution bathing the patch. A series of applications of 300 μM ACh (200 ms) was first applied to the patch. We then recorded the responses following different protocols: (+/−) protocol: the patch was exposed 2 min to bath solution containing a specified concentration of CrV and then a 200 ms pulse of 300 μM ACh was applied; (+/+) protocol: 2-min exposure to bath solution containing a specified concentration of CrV followed by a 200 ms pulse of bath solution containing ACh plus the same concentration of CrV; (−/+) protocol: 200 ms pulse of bath solution containing 300 μM ACh plus CrV without preincubation. After the different application protocols drug-free solutions were applied again to assess loss of channel activity. In some experiments, the preincubation time with CrV varied between 0 and 12 min and currents corresponding to the different preincubation times were recorded from the same patch.

Macroscopic currents were filtered at 5 kHz, digitized at 20 kHz, and stored on the hard disk. Data analysis was performed using the IgorPro software (WaveMetrics Inc., Lake Oswego, OR). The ensemble mean current was calculated for 10 individual current traces. Mean currents were fitted by a single-exponential function:

$$I_{(t)} = I_o^{(-t/\tau_d)} + I_\infty \quad (6)$$

where I_o and I_∞ are the peak and the steady state current values, respectively and τ_d is the decay time constant that measures the current decay due to desensitization. Current records were aligned with each other at the point where the current had risen to 50% of its maximum level. Peak currents corresponded to the values obtained by extrapolation of the decay currents to this point. Fractional inhibition of peak current was calculated as the ratio of the current in the presence of CrV (I_{CrV}) to the current in the absence of the drug (I_{cont}). This ratio was plotted as a function of CrV concentration and the curve was fitted to the Hill equation:

$$I_{CrV}/I_{cont} = IC_{50}^{n_H}/(IC_{50}^{n_H} + [CrV]^{n_H}) \quad (7)$$

where [CrV] is the concentration of CrV, and IC_{50} is the concentration of CrV that produces 50% inhibition of ACh-activated AChR currents.

Single-channel currents were recorded in the cell-attached patch configuration essentially as described before (*23*, *24*). The bath and pipet solutions contained 142 mM KCl, 5.4 mM NaCl, 1.8 mM $CaCl_2$, 1.7 mM $MgCl_2$, and 10 mM HEPES, pH 7.4. Single channel currents were recorded using an Axopatch 200 B patch-clamp amplifier (Axon Instruments, Inc., CA), digitized at 5 μs intervals with the PCI-6111E interface (National Instruments, Austin, TX), recorded to the computer hard disk using the Acquire program (Bruxton Corporation, Seattle, WA), and detected by the half-amplitude threshold criterion using the TAC 4.0.10 program (Bruxton Corporation, Seattle, WA) at a final bandwidth of 10 kHz. Open- and closed-time histograms were plotted using a logarithmic abscissa and a square root ordinate and fitted to the sum of exponential functions by maximum likelihood using the TACFit program (Bruxton Corporation, Seattle, WA). Clusters of openings corresponding to a single channel were identified as a series of closely spaced events preceded and followed by closed intervals greater than a specified duration (τ_{crit}). This duration was taken as the point of intersection of the predominant closed component and the succeeding one in the closed time histogram. For 100 μM ACh, this duration was about 2 ms. Cluster duration histograms were constructed setting the burst resolution time to that corresponding to τ_{crit} (*13*).

Molecular Modeling of the Resting Ion Channel. The full PDB file for the resting state of *Torpedo* AChR (PDB id 2BG9) (*27*) was edited to produce the five M2 α-helices that line the pore of the ion channel from position 0′ (e.g., after the threonine ring) to position 20′ (e.g., the outer or extracellular ring): Lys^{242}-Glu^{262} from both α1 subunits, Lys^{248}-Asp^{268} from the β1 subunit, Lys^{256}-Gln^{276} from the δ

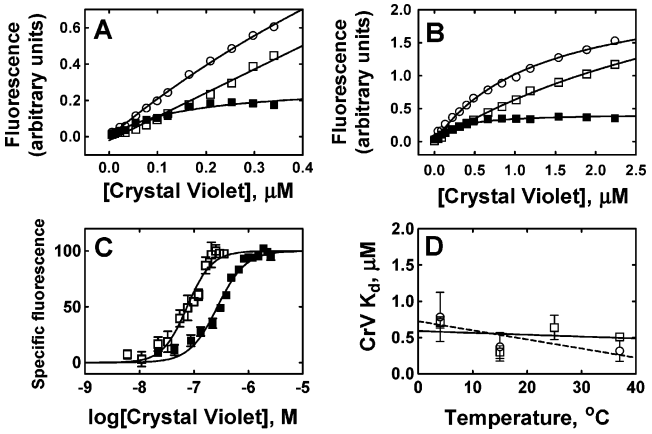

FIGURE 2: Crystal violet binding to AChRs in different conformational states. (A, B) Hyperbolic curves are shown for the total [in the absence of any competitor; (○)], nonspecific [in the presence of the specific competitor; (□)], and specific [total − nonspecific; (■)] CrV fluorescence. CrV was directly titrated into *Torpedo* AChR-containing membranes (0.3 μM) in the presence of 1 mM CCh (desensitized) (A) or in the absence of CCh (resting) (B). Nonspecific binding was determined in the presence of 100 μM PCP (desensitized) or 200 μM tetracaine (resting). Each plot is the average of an experiment in duplicate. (C) PCP-sensitive CrV fluorescence in the resting (■) and desensitized state (□). Estimates of the K_d and n_H values for CrV were determined according to eq 1, and reported in Table 1. (D) Temperature effect on CrV binding to the AChR in the resting (□) and desensitized state (○). The CrV K_d was determined at 5, 15, 25, and 37 °C, respectively. Shown is the mean ± SD from three separate experiments.

subunit, and Lys^{250}-Gln^{270} from the γ subunit. This structure was displayed in the Biopolymer module of Insight 2005 (Accelrys, San Diego, CA) and CrV was built in the same module. CrV was positioned in the center of the pore at the level of the 20′ residues, and the two structures were placed in the center of a 60 × 60 × 60 Å periodic box which was then filled with 6,580 water molecules. The backbone atoms of the pore structure were restrained to their original position with a harmonic force constant of 100 kcal/Å^2, and the whole assembly was optimized to a gradient of 0.1 kcal/Å using the Discover module of Insight 2005 with the Consistent Valence Force Field (CVFF). Then the assembly was relaxed with 25 000 steps of molecular dynamics in the constant number of atoms, volume, and temperature (NVT ensemble) at 400 K and a time step of 1 fs using the same backbone restraints. The entire simulation was repeated with different starting positions of CrV. First, the CrV was moved to the middle of the ion pore (close to position 10′) along the central axis and the simulation was repeated as above. Second, The CrV at position 10′ was rotated 90° and the simulation was repeated as above. Finally, the additional assemblies were reoptimized with the same parameters as above.

RESULTS

Temperature Effect on Crystal Violet Binding. To study the thermodynamic parameters for the AChR−CrV interactions, we first determined the specific CrV fluorescence by direct titrations. In this regard, Figure 2 shows the hyperbolic plots for the total (no competitor added), nonspecific (in the presence of 100 μM PCP), and specific (total − nonspecific) CrV fluorescence in the desensitized (Figure 2A) and in the resting (Figure 2B) state. Subsequently, the PCP-sensitive CrV fluorescence was replotted as a sigmoid curve according to eq 1. Figure 2C shows the respective sigmoid curves for the resting and desensitized state. Then, the respective K_d values for CrV in different conformational states were calculated using eqs 2 and 3. The observed K_d values were 270 ± 12 nM in the resting state and 80 ± 4 nM in the desensitized state (Table 1). A slightly higher value for the resting state (IC_{50} = 0.8 ± 0.2 μM) was obtained using patch-clamp recordings (Figure 8). This indicates that CrV has higher affinity for the desensitized state than that for the resting state. In addition, the observed n_H values were 1.27 ± 0.20 for the desensitized state and 1.32 ± 0.12 for the resting state (Table 1). A similar n_H value (1.3 ± 0.2) was obtained for the resting state using patch-clamp recordings (Figure 8). A n_H value close to one indicates a noncooperative interaction. This suggests that CrV interacts with only one high-affinity binding site on each conformational state in muscle-type AChRs. Our binding affinity and site stoichiometry results were similar to those obtained by Lurtz and Pedersen (*12*).

Table 1: Binding Affinity of Crystal Violet, Tetracaine, and Amobarbital for AChRs in Different Conformational States

ligand	conformational state	K_d[a] or K_i[b]	slope	taken from figure
CrV	desensitized	80 ± 4 nM[a]	1.27 ± 0.20[c]	2A
CrV	resting	270 ± 12 nM[a]	1.32 ± 0.12[c]	2A
tetracaine	resting	1.9 ± 0.5 μM[b]	1.17 ± 0.62[d]	4B
amobarbital	resting	28 ± 20 μM[b]	0.90 ± 0.50[d]	5B

[c] These slopes correspond to the n_H values. [d] These values are the slopes obtained from the respective Schild plots. A slope of one or near unity would indicate a steric mechanism, whereas a slope value far from unity (e.g., <0.5 or >2) would suggest an allosteric-type of inhibition.

CrV interacts with glass and plastic surfaces, precluding the determination of the free concentration. Thus, Lurtz and Pedersen (*12*) used a centrifugation protocol to separate the free from the bound CrV. In contrast to that, we directly titrated CrV into AChR membrane suspensions and determined the specific CrV fluorescence by subtracting the nonspecific fluorescence from the total fluorescence as shown in Figures 2A,B. Although the calculated K_d values for CrV using this protocol were slightly higher than that obtained by Lurtz and Pedersen (*12*), we could distinguish the affinity difference between the resting and the desensitized states (Table 1). Since our method does not need any centrifugation procedure, it is less laborious and time-consuming than the method of Lurtz and Pedersen.

To thermodynamically characterize the CrV binding site, the temperature effect on CrV affinity was studied at 5, 15, 25, and 37 °C. Figure 2D shows the calculated CrV K_d at different temperatures, in either the resting or desensitized state. The data indicate that there is no significant effect produced by temperature changes on CrV affinity. Thus, it was impossible to obtain the thermodynamic parameters, and consequently the thermodynamic characterization of the CrV−AChR interactions could not be achieved. Nevertheless, this temperature-independent behavior is in agreement with previous work showing that the PCP rate constants were temperature independent as well (*28*) (reviewed in ref *29*). The fact that both CrV and PCP present similar thermodynamic properties is another piece of evidence suggesting that these ligands bind to overlapping sites.

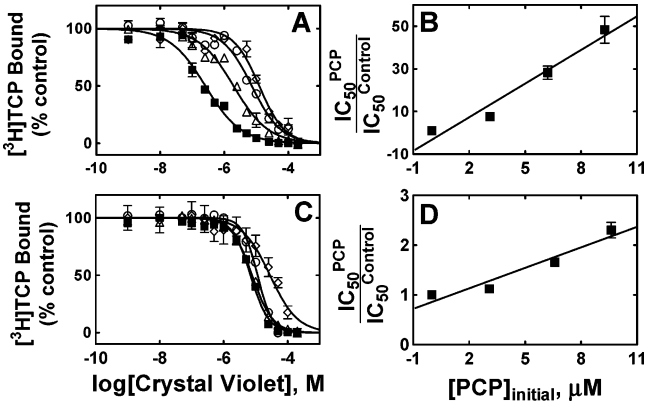

FIGURE 3: Crystal violet-induced inhibition of [^{3}H]TCP binding to desensitized (A) and resting (C) AChRs. AChR-rich membranes (0.3 μM) were equilibrated with ~7 nM [^{3}H]TCP, in the presence of 1 mM CCh (desensitized) or 1 μM α-BTx (resting), at initial PCP concentrations of 0 [control (■)], 3.1 (△), 6.2 (○), and 9.3 μM (◊). Nonspecific binding was obtained in the presence of 100 μM PCP (desensitized) or 200 μM tetracaine (resting). Each plot is the average of two different experiments. The apparent IC_{50} values were calculated by nonlinear least-squares fit according to eq 2. (B, D) Modified Schild plots for CrV-induced inhibition of [^{3}H]TCP binding in the desensitized (B) and resting state (D), respectively. Both plots show a linear relationship with r^2 values of 0.93 and 0.91, respectively, suggesting that CrV inhibits [^{3}H]TCP binding by a steric mechanism in both states.

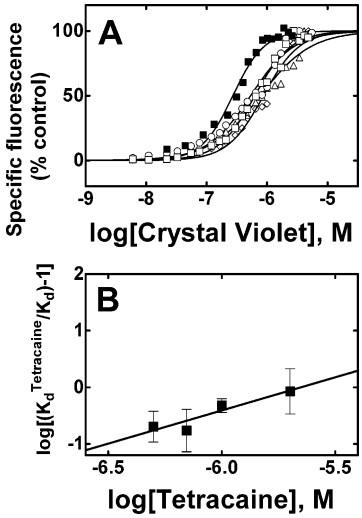

FIGURE 4: Effect of tetracaine on CrV binding to the restingAChR. (A) Specific CrV fluorescence in the presence of different concentrations of tetracaine. CrV was directly titrated into *Torpedo* AChRs (0.3 μM) in the resting state (no CCh), in the presence of different concentrations of tetracaine: 0 [control (■)], 0.5 (□), 0.7 (○), 1 (◊), and 2 μM (△). Nonspecific binding was obtained in the presence of 200 μM tetracaine or alternatively 100 μM PCP. The apparent IC_{50} values were calculated by nonlinear least-squares fit according to eq 2. The apparent K_i values were calculated using eq 3. (B) Schild plot for tetracaine-induced inhibition of CrV binding to resting AChRs was determined according to eq 4. Shown is the mean ± SD from at least three separate experiments. A linear relationship with a slope of 1.17 ± 0.62 was observed. The K_i value for tetracaine was graphically calculated as the antilog of the *x*-intercept (when $y = 0$), and summarized in Table 1.

Schild Plot Analyses for Crystal Violet Binding to the PCP Site. To localize the CrV binding site, we determined the CrV-induced inhibition of [^{3}H]TCP binding in the resting and desensitized state. CrV completely eliminated specific [^{3}H]TCP binding in a concentration-dependent fashion in either the desensitized (Figure 3A) or the resting state (Figure 3C). The calculated n_H values are not close enough to unity (0.78 ± 0.06 and 1.40 ± 0.09, respectively) to assert that CrV inhibits [^{3}H]TCP binding in a noncooperative manner. Thus, we cannot rule out that this competition is produced by a potent allosteric mechanism. In this regard, we determined whether CrV inhibits [^{3}H]TCP binding in a steric or allosteric manner by Schild-type analyses. Figure 3A,C shows the CrV-induced inhibition of [^{3}H]TCP binding at different initial concentrations of PCP, in the desensitized and resting state, respectively. At increased initial PCP concentrations, the plots were shifted to the right. This indicates that at increased PCP concentrations, higher CrV amounts are required to inhibit the binding of [^{3}H]TCP + PCP (see Figure 3A,C). Using the apparent IC_{50} values (at increased initial PCP concentrations) obtained from these figures, we constructed the respective modified Schild plots for the desensitized (see Figure 3B) and resting AChR (see Figure 3D). These modified Schild plots show a linear relationship with goodness-of-fit values (r^2) of 0.93 (Figure 3B) and 0.91 (Figure 3D), suggesting that CrV inhibits [^{3}H]TCP binding by a steric mechanism. Thus, we infer that the CrV binding site overlaps the PCP locus in the desensitized state as well as in the resting state.

Schild Plot Analyses in the Resting State. Our previous results have shown that the tetracaine binding site bridges both the PCP and the barbiturate sites in the resting state (*10*, *11*, *30*) (reviewed in refs *7* and *8*). In addition, the molecular volume for CrV (461 Å^3) is larger than that for PCP (311 Å^3) (*10*). Thus, it is possible that the CrV molecule may extend deeper in the resting ion channel to reach the barbiturate locus as well. In this regard, we studied the interaction of CrV with either the tetracaine or the barbiturate binding site by determining the apparent K_d of CrV in the presence of different concentrations of tetracaine or barbiturates (e.g., amobarbital and pentobarbital). Figures 4A and 5A display the effect of increasing concentrations of tetracaine or amobarbital, respectively, on CrV binding. In Figure 4A, it can be seen that at increased tetracaine concentrations plots shifted to the right, yielding increased apparent K_d values for CrV. The observed apparent K_d's were replotted according to the Schild equation (eq 4). The Schild plot (Figure 4B) shows a linear relationship with a slope of 1.17 ± 0.62 (Table 1). Although the slope is close to unity, suggesting that tetracaine interacts with the CrV binding site in a steric manner, the standard deviation value does not allow us to rule out a potent allosteric mechanism. The calculated K_i value for tetracaine was 1.9 ± 0.5 μM (Figure 4B; Table 1). This value is in the same range as that obtained by tetracaine-induced inhibition of [^{3}H]TCP binding experiments (*11*). Taking into account these results, the previous Schild plot analysis for CrV-induced inhibition of [^{3}H]TCP in the resting state (Figure 3D), and the information that PCP partially overlaps the tetracaine domain (*10*, *11*) (reviewed in refs *7* and *8*), we suggest that CrV binds the tetracaine domain by overlapping the PCP locus.

We further studied the change in the apparent K_d for CrV at increasing initial concentrations of amobarbital. In Figure 5A, it can be seen that the plots shifted to the right at augmented amobarbital concentrations, yielding increased apparent K_d values for CrV. Schild plot results (see Figure 5B) show a linear correlation with a slope of 0.90 ± 0.50 μM and a K_i of 28 ± 20 μM for amobarbital (Table 1).

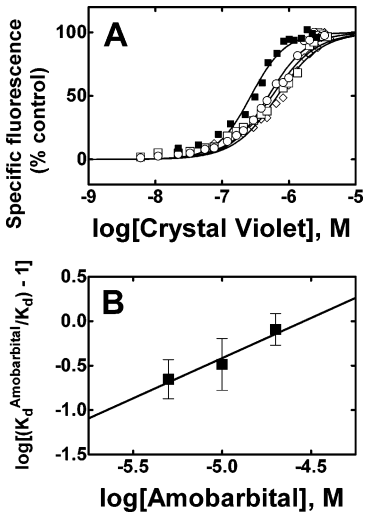

FIGURE 5: Effect of amobarbital on CrV binding to the restingAChR. (A) Specific CrV fluorescence in the presence of different concentrations of amobarbital. CrV was directly titrated into *Torpedo* AChRs (0.3 μM) in the resting state (no CCh), in the presence of different concentrations of amobarbital: 0 [control (■)], 5 (○), 10 (□), and 20 μM (◊). Nonspecific binding was obtained in the presence of 200 μM tetracaine. The apparent IC_{50} values were calculated by nonlinear least-squares fit according to eq 2. The apparent K_i values were calculated using eq 3. (B) Schild plot for amobarbital-induced inhibition of CrV binding to resting AChRs was determined according to eq 4. Shown is the mean ± SD from at least three separate experiments. A linear relationship with a slope of 0.90 ± 0.50 was observed. The K_i value was graphically calculated as the antilog of the *x*-intercept (when $y = 0$), and summarized in Table 1.

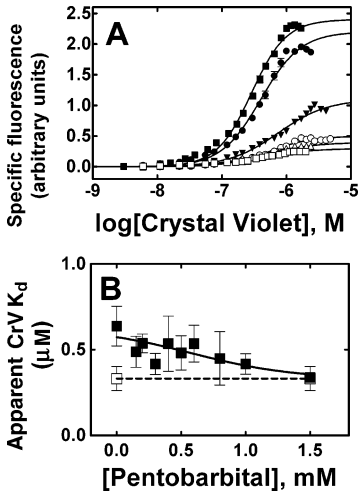

FIGURE 6: Pentobarbital-induced modulation of CrV binding to the resting AChR. (A) Specific CrV fluorescence in the presence of different concentrations of pentobarbital. CrV was directly titrated into *Torpedo* AChRs (0.3 μM) in the resting state (no CCh), and in the presence of different concentrations of pentobarbital: 0.2 (△), 0.5 (○), 0.8 (▼), and 1.5 mM (●). Nonspecific binding was obtained in the presence of 200 μM tetracaine. For comparative purposes, the PCP-sensitive CrV fluorescence, in the absence of pentobarbital, in the resting (□) and desensitized state (■) were also included. Shown is the average from experiments performed in duplicate. (B) Apparent K_d's for CrV at different concentrations of pentobarbital in the resting state (■). The CrV K_d in the desensitized state (□) (without pentobarbital) is included only for comparative purposes. The apparent K_d values from Figure 6A as well as from additional experiments were calculated using eq 1. Shown is the mean ± SD from at least three separate experiments. The following relationship was observed: CrV K_d values decrease at higher pentobarbital concentrations, suggesting a pentobarbital-induced AChR desensitization process.

Although the slope was close to unity, the obtained K_i value was higher when compared to the K_d (3.7 ± 0.7 μM) obtained by [^{14}C]amobarbital equilibrium binding to the resting AChR (*30*). However, given the error estimate, we cannot conclude that the calculated K_i value is significantly different from the [^{14}C]amobarbital K_d.

We also studied the effect of a barbiturate analogue that binds with low affinity to the AChR in the resting state (*30*). Thus, we determined the effect of increasing concentrations of pentobarbital in the millimolar range on CrV binding. Figure 6A shows the change in PCP-sensitive CrV fluorescence at increasing concentrations of pentobarbital. For comparative purposes, the CrV-specific fluorescence in the resting and desensitized state, in the absence of pentobarbital, were also included. As the pentobarbital concentration was increased, the AChR-bound CrV fluorescence was augmented, reaching levels comparable to those obtained in the desensitized state. Figure 6B shows the respective K_d values calculated from Figure 6A according to eqs 2 and 3, as well as additional K_d values obtained at different concentrations of pentobarbital. This plot shows an interesting correlation: lower CrV K_d values are obtained at increased pentobarbital concentrations. This could be due to two possible mechanisms: (i) high concentrations of pentobarbital induced AChR desensitization and subsequently the CrV specific fluorescence is increased, and/or (ii) the barbiturate induced local conformational changes in the proper CrV binding site, increasing the affinity of the fluorophor. To distinguish between these two possible mechanisms, we determined the specific florescence of CrV in the presence of 1.5 mM pentobarbital. We measured fluorescence when the AChR was in the resting but activatable state (no α-BTx) or when it was arrested in the resting state (in the presence of α-BTx) (*17*). Our results (data not shown) indicate that the maximal specific florescence of CrV in the presence of both pentobarbital and α-BTx was lower than that in the absence of α-BTx. These data support the idea that pentobarbital induced AChR desensitization, enhancing concomitantly the CrV affinity for the AChR. If the other mechanism had taken place, we should have observed an increase of CrV affinity, even in the presence of α-BTx. Thus, we can rule out the possibility that barbiturates at high concentrations induce local conformational changes in the proper CrV binding site but confirm that the CrV affinity is enhanced by a pentobarbital-induced AChR desensitization process. High pentobarbital concentrations may induce AChR desensitization by binding to low-affinity sites at the lipid−protein interface (*30*). These results support the proposal that barbiturates modulate CrV binding in an allosteric fashion. This modulatory process is inconsistent with barbiturates inhibiting CrV binding by a steric mechanism.

Crystal Violet-Induced AChR Desensitization. To determine if CrV induced AChR desensitization, we studied the effect of CrV on the binding of the fluorescent agonist DTMA. Figure 7 shows that CrV in the low concentration range enhanced the DTMA specific fluorescence by ∼70%. Previous experiments using [^{3}H]ACh as the agonist probe showed that CrV increased the agonist affinity by ∼10-fold (*12*). The difference in the extent of binding increase might be due to the type of agonist used since the susceptibility to affinity changes for the fluorescent agonist (e.g., DMTA)

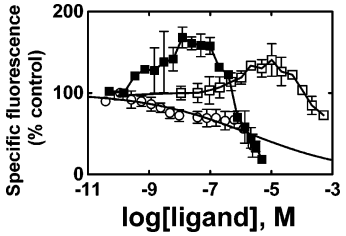

FIGURE 7: CrV-induced modulation of the binding of the fluorescent agonist DTMA. CrV was directly titrated into *Torpedo* AChR membranes (0.3 μM), in the presence of 6 μM DTMA, in the resting but activatable [in the absence of α-BTx; (■)] or in the desensitized state [in the presence of 200 μM proadifen; (○)]. The effect of the local anesthetic proadifen on DTMA binding is also included as a control (□). Shown is the mean ± SD of experiments performed in triplicate. The apparent $ED_{50}^{R\rightarrow D}$ and IC_{50} values as well as the respective n_H's were calculated by nonlinear least-squares fit according to eq 2, and summarized in Table 2.

Table 2: Modulatory Effect of Crystal Violet and Proadifen on the Binding of the Fluorescent Agonist Dansyltrimethylamine (DTMA)[a]

ligand	$EC_{50}^{R\rightarrow D}$, nM	IC_{50}, μM
CrV	1.4 ± 0.9	0.76 ± 0.08
proadifen	530 ± 280	640 ± 180

[a] Data were obtained from Figure 7.

could be distinct to that for the radiolabeled agonist (e.g., [^{3}H]ACh). The fact that proadifen enhanced DTMA specific fluorescence by ~50% (Figure 7) supports this possibility. The calculated CrV concentration required to produce 50% AChR desensitization ($EC_{50}^{R\rightarrow D}$) is in the nanomolar concentration range (Table 2). This is in accord with the fact that CrV binds with high affinity (Figure 2B) (also see ref *12*). It also indicates that the fluorophor is a potent desensitizing agent. At higher concentrations, however, CrV inhibits DTMA binding to the AChR agonist sites in the submicromolar concentration range (0.76 ± 0.08 μM; Table 2), probably by a steric mechanism. This result is also consistent with the data from Lurtz and Pedersen (*12*).

As a control experiment, we observed the effect of CrV on DTMA specific fluorescence in the already desensitized AChR (in the presence of 200 μM proadifen). As was expected, CrV did not produce any additional increase in DTMA fluorescence (see Figure 7). Nevertheless, a slight decrease in the specific DTMA fluorescence was observed at all CrV concentration ranges.

For the sake of comparison, Figure 7 shows that proadifen at low concentrations also enhanced DTMA specific fluorescence. This is in accord with previous results indicating that this local anesthetic desensitizes the AChR (*21*). Interestingly, proadifen produced desensitization at a concentration range ~370 times higher than that for CrV (Table 2). At higher concentrations, however, proadifen inhibited DTMA binding to the agonist sites. The observed high IC_{50} value (>600 μM; Table 2) indicated that, in fact, proadifen binds with very low affinity to the AChR agonist sites, according with the definition of NCAs (reviewed in refs *6* and *29*). These results are consistent with previous experiments using [^{3}H]ACh as the agonist probe (*12*).

Effects of Crystal Violet on Macroscopic and Single-Channel Currents. To determine the mechanism of ion channel inhibition by CrV, we studied the effect of the drug on macroscopic currents recorded from outside-out patches

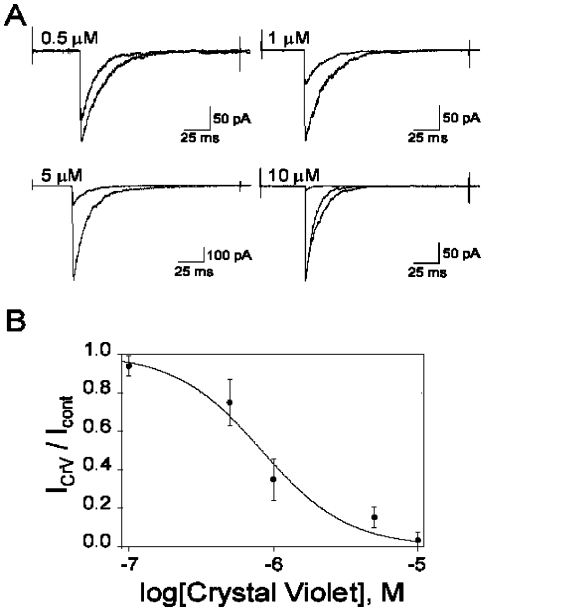

FIGURE 8: Effects of CrV on macroscopic currents activated by 300 μM ACh. (A) Ensembled mean currents obtained in the absence and continuous presence of 0.5, 1.0, 5.0, and 10.0 μM CrV [(+/+) protocol]. The time of preincubation with CrV was 2 min. To illustrate recovery after CrV application, the recovery current after a 10 μM CrV application is shown. (B) Inhibition of peak currents as a function of CrV concentration. Peak currents in the presence of CrV are normalized to control currents. Each point represents the mean ± SD of at least three measurements. Data are fit to the Hill equation (eq 7) and the fitting parameters were IC_{50} = 0.8 ± 0.2 μM and n_H = 1.3 ± 0.2.

rapidly perfused with 300 μM acetylcholine (ACh). We first evaluated how the macroscopic currents were modified by 2 min preincubation with CrV followed by application of ACh containing CrV [(+/+) protocol, see Experimental Procedures]. In all these experiments, the control current was recorded before and after each application protocol. As shown in Figure 8A, CrV decreased the peak current as a function of the CrV concentration. Recovery of the initial control current after CrV application was higher than 90% for all concentrations (Figure 8A), indicating a reversible effect of CrV on AChR. The decay time constant (τ_d) was not affected by the presence of 0.5−5.0 μM CrV. For instance, τ_d was 16.8 ± 5.0 ms for control currents and 15.2 ± 4.0 ms for 5.0 μM CrV. From the relationship between the decrease in peak current and drug concentration, an IC_{50} value of 0.8 ± 0.2 μM (n_H = 1.3 ± 0.2) was obtained (Figure 8B). The main conclusion from these experiments is that CrV decreases peak currents without affecting rapid desensitization from the open state.

We also evaluated how the macroscopic current was modified by the different application protocols. To this end, patches were exposed to 1 μM CrV before (±), during (−/+), or before and during the activation by ACh (+/+) (see Experimental Procedures). Figure 9A shows ensemble currents for the different application protocols. The fact that the current was not affected in the −/+ protocol and that the changes were similar in the +/− and in the +/+ protocol indicated that preincubation with the drug was necessary and sufficient for the inhibition of the peak current. In this regard, the observed IC_{50} value for CrV would correspond to the inhibition of the ion channel opening by previously acting on the resting state. To determine the effect of the time of

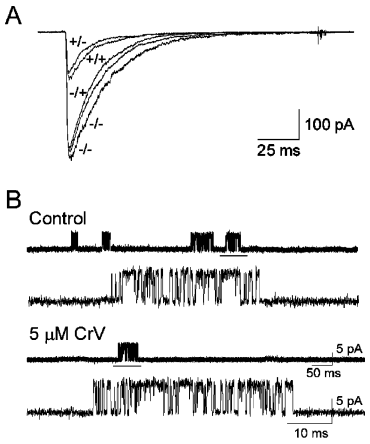

FIGURE 9: Inhibition of AChR current as a function of application protocol. (A) AChR are activated by 300 μM ACh, and 1 μM CrV is applied in different protocols: (−/−) protocol: control currents; (±) protocol: 2 min preincubation with CrV and activation with ACh alone; (−/+) protocol: activation with a solution containing ACh and CrV without preincubation; and (+/+) protocol: 2 min preincubation and activation of currents in the presence of CrV. (B) Single-channel traces of AChR activated by 100 μM ACh in the absence (control) and presence of 5 μM CrV. Channels are shown as upward deflections. Traces are shown at two different time scales for each condition. Filter: 9 kHz. Membrane potential: −70 mV.

preincubation on the decrease of the peak current, we recorded every 2 min currents from the same patch preincubated with CrV from 0 to 12 min (+/− protocol). In our system, the complete exchange of the bath solution with that containing CrV was achieved after 30−50 s. No differences in the decrease of the peak currents were observed between 2 and 12 min of preincubation. The observed I_{CrV}/I_{cont} values were 0.58 ± 0.07 (2 min), 0.50 ± 0.09 (4 min), 0.53 ± 0.04 (8 min), and 0.51 ± 0.08 (12 min). These results confirmed that the maximal effect was achieved in less than 2 min of exposure to CrV.

Since CrV also competes for the *Torpedo* AChR agonist binding sites (*12*) (see also Figure 7), we investigated if the reduction in peak current was due to the competitive action of CrV. To this end, we activated AChR with a solution containing 100 μM ACh and high concentrations of CrV [protocol (−/+)]. The peak current did not decrease in the presence of 1 μM CrV but slightly decreased to 0.92 and 0.90 in the presence of 10 and 100 μM CrV, respectively. Thus, our result indicated that a competitive antagonism was not responsible for the reduction in the peak current at concentrations of CrV lower than 100 μM. Nevertheless, at higher concentrations, CrV seemed to act as a competitive antagonist. CrV started to act as a competitive antagonist at different concentration ranges between these results in mouse muscle (Figure 9A) and those in *Torpedo* AChRs (Figure 7; Table 2). These differences could be related to the different receptor subtype. An alternative explanation could be due to different relationships between binding affinity and efficacy to inhibit the current.

To further explore the inhibitory mechanism elicited by CrV on the AChR, we recorded single channel currents activated by 100 μM ACh in the absence and in the presence of 5 μM CrV (Figure 9B). At this ACh concentration, activation takes place in clear clusters. Each activation period (cluster) begins with the transition of a single receptor from

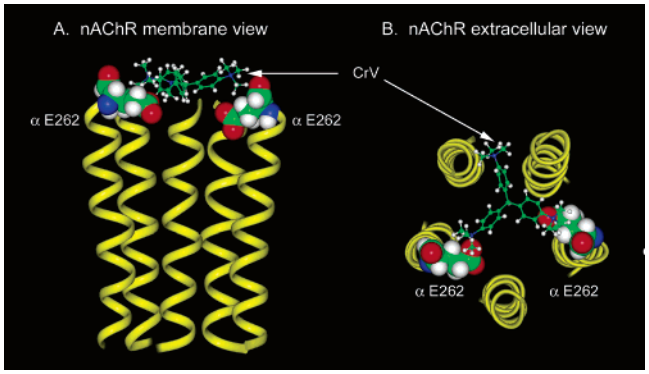

FIGURE 10: Molecular modeling of the *Torpedo* AChR ion channel in the resting (closed) state complexed with CrV. The model was constructed using Unwin's model (PDB id 2BG9) (*26*). This structure was displayed in the Biopolymer module of Insight 2005 (Accelrys, San Diego, CA) and CrV was built in the same module. CrV was positioned in the center of the pore at the level of the 20′ residues, and the two structures were placed in the center of a 60 × 60 × 60 Å periodic box which was then filled with 6580 water molecules. The backbone atoms of the pore structure were restrained to their original position with a harmonic force constant of 100 kcal/Å^2, and the whole assembly was optimized to a gradient of 0.1 kcal/Å using the Discover module of Insight 2005. Then the assembly was relaxed with 25 000 steps of molecular dynamics at 400 K and a time step of 1 fs using the same backbone restraints. The entire simulation was repeated with different starting positions of CrV. First, the CrV was moved to the middle of the ion pore (close to position 10′) along the central axis and the simulation was repeated as above. Second, The CrV at position 10′ was rotated 90° and the simulation was repeated as above. Finally, the assembly was reoptimized with the same parameters as above.

the desensitized to the activatable state and terminates by returning to the desensitized state (*13*, *26*). In the absence of CrV, the duration of the main open and closed components within clusters is 0.97 ± 0.06 ms and 0.29 ± 0.05 ms, respectively. The mean cluster duration is 38 ± 15 ms, and the probability of channel opening (P_{open}) within a cluster is 0.75 ± 0.05 (n = 3). In the presence of 100 μM ACh and 5 μM CrV, very low channel activity is observed. However, activation occurs also in clusters. No changes are observed in the cluster properties with respect to the control. The mean open, mean closed, mean cluster duration, and P_{open} values are 0.98 ± 0.15 ms, 0.21 ± 0.05 ms, 42 ± 13 ms, and 0.77 ± 0.06, respectively (n = 3). This result shows that CrV does not affect significantly the gating kinetics and does not act on open channels. In addition, it supports an increase of desensitization from the resting state, as suggested by the macroscopic current recording experiments.

Molecular Modeling of the CrV Binding Site in the Resting Ion Channel. Using the molecular model of the *Torpedo* AChR in the resting state (PDB id 2BG9) (*27*), CrV docking in the ion pore was performed in a periodic box of water to simulate binding in solution. As a result, electrostatic interactions are more realistic because of solvation of the charged moieties. Nevertheless, two of the charged amino groups of CrV moved into van der Waals contact with the two α1-Glu^{262} residues (E^{262}) located in the outer or extracellular ring (e.g., position 20′) of the ion pore. Figure 10 shows the molecular modeling of the resting ion channel and the potential binding site location for CrV obtained by molecular dynamics. The third charged group of CrV was solvated by water molecules. These water molecules also filled the pore and moved above and below the CrV

molecule. The position of CrV in the ion pore of AChR shows that it is plausible for this molecule to diffuse down the pore and act as a steric channel blocker. CrV returned to essentially the same final position after starting from three distinctly different initial configurations, supporting the observed location (Figure 10). However, it is possible that the molecule would bind to other positions along the *z*-axis of the pore if the simulation were run longer or with more flexibility allowed in the harmonic restraint of the backbone atoms of the residues. Our experiments indicating that CrV binding was not affected by temperature changes (see Figure 2D) also suggested that the molecular dynamics results would not be different at higher temperatures.

DISCUSSION

This study was an attempt to determine the molecular mechanisms and the binding site location for the fluorophor CrV, a high-affinity NCA of the AChR (*12*). To determine the CrV binding site location, we used radiolabeled competition binding experiments (e.g., CrV-induced inhibition of [^{3}H]TCP binding), fluorescence titrations (e.g., tetracaine and amobarbital-induced inhibition of AChR-bound CrV fluorescence). The results were analyzed according to Schild (*19*). Patch-clamp recordings (e.g., CrV-induced inhibition of AChR macrocurrents) and fluorescent assays (e.g., CrV-induced modulation of AChR-bound DMTA fluorescence) were also applied to determine the molecular mechanisms underlying the noncompetitive inhibition provoked by CrV.

Localization of the Crystal Violet Binding Site in Different Conformational States. The results from the equilibrium binding experiments using fluorescence spectroscopy and patch-clamp recordings demonstrated that CrV binds to a PCP-sensitive site in the muscle-type AChR and that the fluorophor prefers the desensitized to the resting conformational state (Table 1; Figure 8B). The radiolabeled competition experiments performed in parallel indicated that CrV inhibited the binding of [^{3}H]TCP, the structural and functional analogue of the hallucinogen and general anesthetic PCP, to the desensitized and resting AChRs with n_H values close to unity (Figure 3A,C). This result is in accord with our fluorescence titrations (Table 1) and patch-clamp recordings (Figure 8B) in which the n_H values were also close to unity. Hill coefficients close to unity indicated a noncooperative interaction between CrV and PCP, suggesting that CrV interacted with only one binding site on each AChR conformational state. This conclusion supports previous data (*12*). However, we cannot predict whether the location for the CrV binding site was the same or distinct in each conformational state. The fact that CrV binds to just one locus is in agreement with previous evidence indicating that there exists one high-affinity PCP binding site on each AChR conformational state (*10*, *11*) (reviewed in refs *7* and *8*). Although this and previous (*12*) evidence suggests a steric mode of competition between CrV and PCP, the possibility that CrV inhibits [^{3}H]TCP binding by a potent allosteric mechanism cannot be ruled out. To clarify this point, we used Schild-type analyses. Our results indicate that in fact CrV displaces [^{3}H]TCP binding from its high-affinity site in the desensitized as well as in the resting AChR by a steric mechanism (Figure 3B,D). Subsequently, this experimental evidence suggests that the CrV binding site overlaps the PCP locus in the resting as well as in the desensitized state. This evidence supports previous data (*12*).

Previous studies aimed at characterizing the PCP locus were only partially successful (reviewed in refs *4*, *6*−*8*, *29*). For instance, early photoaffinity labeling experiments using [^{3}H]azido-PCP as a probe for the PCP site only demonstrated that a proteolytic fragment containing the transmembrane segments M1, M2, and M3 from the α1 subunit was labeled in the desensitized and resting AChR (*31*). More recent photoaffinity labeling studies using [^{3}H]ethidium diazide, which binds with high affinity to the PCP locus, helped to determine the structural components of this site in the desensitized state (*32*) (reviewed in ref *7*). The results indicated that residues Leu^{251} at position 9′ (e.g., the leucine ring) and Ser^{252} at position 10′ from the α1-M2 transmembrane segment as well as other unknown amino acids located in the M1 and M2 transmembrane segments from the δ subunit are structurally involved in this particular site.

The knowledge of the PCP and ketamine (a hallucinogen and general anesthetic with similar pharmacological properties as PCP) binding sites in the resting and open states is less than that in the desensitized state. Site-directed mutagenesis studies determined that the PCP binding site in the open ion channel includes residues located at position 6′ (e.g., the conserved serine ring), 8′ and 10′ (both are located one amino acid apart from the conserved leucine ring) from the M2 transmembrane segment (*33*) (reviewed in ref *34*). In addition, we suggested that the PCP binding site in the resting state is located more extracellularly than that in the desensitized and open state, probably close to the mouth of the external vestibule (*10*, *11*) (reviewed in refs *7* and *8*). Interestingly, a single amino acid (e.g., Ala^{258}), located at position 19′ in the extracellular portion of the M2 transmembrane segment, was found to be responsible for the pharmacological properties of ketamine on the α7 AChR (*35*). This suggests that different AChR subtypes or conformation states may have the PCP/ketamine binding site located in distinct domains. We also speculated that the aromatic tertiary amino group from the PCP (or TCP) molecule (see Figure 1) might interact with acidic residues (e.g., α1-Glu^{262}) located at position 20′ (e.g., the outer or extracellular ring) (*10*, *11*) (reviewed in refs *7* and *8*). Considering our findings that CrV sterically binds to the PCP locus in the resting state (Figure 3D), we suggest that the tertiary amino groups from the CrV molecule (see Figure 1) can also be responsible for the binding to α1-Glu^{262} by charge interactions. The CrV molecule has three tertiary amino groups (one on each aromatic ring; see Figure 1) that are positively charged at physiological pH. On the other hand, there are two Glu^{262} residues (one on each α1 subunit) containing one carboxylate group per each amino acid that are negatively charged at physiological pH. One possibility is that two of the CrV amino groups interact with the two carboxylate groups. Figure 10 shows the molecular modeling of the *Torpedo* ion channel in the resting state, as well as the interactions between two CrV amino groups and the α1-Glu^{262} carboxylate moieties obtained by molecular dynamics. The fact that, in the resting state, CrV presents 3-fold higher affinity (K_d = 0.27 μM; Table 1) than [^{3}H]TCP (K_d = 0.83 μM; *10*), a molecule with only one tertiary aromatic amino group, supports such charge interactions. Although additional hydrophobic interactions might also take place between the

three aromatic rings from CrV (see Figure 1) and other hydrophobic amino acids located close enough to the external mouth of the resting ion channel, molecular dynamics results do not show these potential interactions (see Figure 10).

Additional experimental results indicate that the PCP locus partially overlaps the tetracaine domain but not the barbiturate or the trifluoromethyliodophenyldiazirine (TID) binding site in the resting state (*10*, *11*, *30*, *36*). On the basis of photoaffinity labeling results, the tetracaine binding site has been located in a long portion of the M2 transmembrane domain that involves residues from position 5′ to 13′ (e.g., the valine ring) (*37*, *38*) and probably extending to the outer ring (position 20′) (*11*). The tetracaine binding site partially overlaps the barbiturate locus in approximately the middle of the ion channel (between position 9′ and 13′) (*30*). In this regard, our fluorescence competition experiments in the resting state indicated that tetracaine (Figure 4A) as well as amobarbital (Figure 5A) inhibits CrV binding to the resting AChR. Schild-type analyses were not conclusive for determining the nature (steric versus allosteric) of the inhibitory mechanism. Nevertheless, the fact that pentobarbital does not decrease, but increases, AChR-bound CrV fluorescence (Figure 6A) supports an allosteric mode of action between barbiturates and CrV and does not support any steric interaction between both drugs. These results suggest that, in the resting ion channel, CrV binds to a portion from the tetracaine domain that comprises the PCP but not the barbiturate binding site. Although the molecular volume for CrV (461 Å^3) is large enough to occupy a deeper location within the resting ion channel, probably overlapping the barbiturate locus, molecular dynamics results indicate that CrV does not interact with the barbiturate locus (see Figure 10). These molecular dynamics results are also in agreement with our conclusion that CrV overlaps both the PCP and the tetracaine binding site. All this evidence supports the idea that the resting ion channel cannot accommodate two charged molecules at the same time (e.g., tetracaine and CrV) but could accommodate one charged (e.g., CrV or PCP) and another uncharged (e.g., TID or barbiturates) ligand (*36*).

Mechanisms of Inhibition Produced by CrV. To further explore the molecular mechanism of AChR inhibition by CrV, we analyzed the changes of ACh-activated macroscopic and single-channel currents in the presence of CrV. The main effect of CrV is a dose-dependent decrease of AChR macroscopic currents without affecting the rate of current decay due to desensitization. Our application protocol (Figure 9A) allowed us to determine that preincubation was necessary and sufficient for CrV to act on AChRs. When CrV was applied simultaneously with ACh, no changes in the peak currents were observed. Therefore, our results indicate that CrV inhibits activation from the resting state of the receptor without affecting the open state. However, this result cannot discard the possibility that CrV also binds to the open state. If this were the case, either the binding or the inhibition rates from this state should be slower than those of desensitization ($\tau_d \sim 16$ ms).

Thus, the observed IC_{50} value for the inhibition of ACh-induced AChR currents would represent the action of CrV on the resting ion channel, precluding the opening of the pore (Figure 8B). This value is consistent with the observed CrV high affinity for the resting AChR (Table 1).

Scheme 1

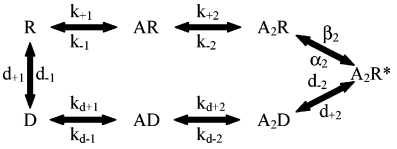

To describe the noncompetitive inhibitory mechanism of CrV, we used the classical scheme for activation and desensitization of AChR (Scheme 1). Here, R represents the resting state, A_2R the di-liganded receptor, A_2R^* the open, and D the desensitized state.

The fact that the probability of channel opening within a cluster, as well as the mean open and closed channel durations, remained constant in the presence of CrV strongly suggests that the drug is not affecting gating kinetics (R to A_2R^* transitions in Scheme 1). In addition, the fact that the decay rate of macroscopic currents, as well as the duration of clusters elicited by high ACh concentrations remain constant in the presence of CrV indicates that the rate of desensitization from the open state (A_2R^* to A_2D in Scheme 1) is not affected. However, it could be possible that CrV stabilizes the A_2D state once this conformational state is reached, in accordance with the fluorescence measurements (see Figure 7). This effect cannot be detected from the present electrophysiological experiments.

An open-channel blocking mechanism has been suggested for CrV (*12*). However, CrV is not acting as an open-channel blocker at the concentrations here tested. If this were the case, changes in current decay rate and in the mean open duration should be expected (*39*−*41*).

The inhibition of the peak current could be due to increased desensitization from the resting (closed) channels or stabilization of preexisting desensitized receptors. These conditions may lead to a shift of the equilibrium population of AChRs to the desensitized state. Taking into account that CrV binds to both resting and desensitized AChRs (Figure 2; Table 1) and that the proportion of desensitized AChRs in the absence of ACh is only 0.01% for the mouse muscle AChR (*42*), we can suggest that CrV stabilizes the already desensitized AChR and increases the conversion from resting to desensitized AChRs. In this regard, we can conclude that CrV changes the proportion between the low-affinity resting state receptors (R) and the high-affinity desensitized state receptors (D) (R to D transition in Scheme 1). This would lead to an increase in agonist affinity and a decrease in the fraction of activatable receptors. In accordance with this suggestion, NCAs such as histrionicotoxin and dibucaine have been shown to increase the allosteric equilibrium constant between desensitized and resting unliganded AChRs (*42*). From our results, it is not possible to determine if the high-affinity state induced by CrV corresponds to the full desensitized receptor (D) or to an intermediate state between resting and desensitized receptor, which has been observed for other NCAs (*26*, *43*). Thus, results from the electrophysiological experiments are not compatible with an open-channel block mechanism and support an allosteric process to explain the action of CrV.

On the other hand, our modeling studies indicate that the CrV binding site is located at the extracellular mouth of the ion channel (see Figure 10). To correlate the functional with the structural results, we propose an allosteric mode of action

for CrV where the fluorophor first binds to the channel mouth when the receptor is in the resting state, and this interaction leads to either an inhibition of channel opening or an increase of desensitization, together with a stabilization of the desensitized state.

This study indicates that CrV is an excellent probe that can be used to characterize the PCP/ketamine binding site in the resting, open, and desensitized states by fluorescence spectroscopy. For instance, fluorescence resonance energy transfer experiments can be planned to determine the distance between the CrV (PCP/ketamine) binding site and other ligand loci. This technique could finally resolve the binding site topology for the AChR. From the therapeutic point of view, clinically important compounds, such as antidepressants (*13*), anti-Parkinson drugs (e.g., adamantane derivatives) (*10*), and drugs for Alzheimer's disease (e.g., anabaseine analogues) (*14*), bind to the PCP/CrV locus, emphasizing the importance of this binding site.

REFERENCES

1. Connolly, C. N., and Wafford, K. A. (2004) The Cys-loop superfamily of ligand-gated ion channels: the impact of receptor structure on function, *Biochem. Soc. Trans. 32*, 529−534.
2. Lester, H. A., Dibas, M. I., Dahan, D. S., Leite, J. F., and Dougherty, D. A. (2004) Cys-loop receptors: new twists and turns, *Trends Neurosci. 27*, 329−336.
3. Hogg, R. C., Raggenbass, M., and Bertrand, D. (2003) Nicotinic acetylcholine receptors: from structure to brain function, *Physiol. Biochem. Pharmacol. 147*, 1−46.
4. Arias, H. R. (2000) Localization of agonist and competitive antagonist binding sites on nicotinic acetylcholine receptors, *Neurochem. Int. 36*, 595−645.
5. Lloyd, G. K., and Williams, M. (2000) Neuronal nicotinic acetylcholine receptors as novel drug targets, *J. Pharmacol. Exp. Ther. 292*, 461−467.
6. Arias, H. R. (1998) Binding sites for exogenous and endogenous noncompetitive inhibitors of the nicotinic acetylcholine receptor, *Biochim. Biophys. Acta Rev. Biomembr. 1376*, 173−220.
7. Arias, H. R., Kem, W. R., Trudell, J. R., and Blanton, M. P. (2002) Unique general anesthetic binding sites within distinct conformational states of the nicotinic acetylcholine receptor, *Int. Rev. Neurobiol. 54*, 1−50.
8. Arias, H. R., and Bhumireddy, P. (2005) Anesthetics as chemical tools to study the structure and function of nicotinic acetylcholine receptors, *Curr. Prot. Peptide Sci. 6*, 451−472.
9. Pagán, O. R., Eteroviæ, V. A., García, M., Vergne, D., Basilio, C. M., Rodríguez, A. D., and Hann, R. M. (2001) Cembranoid and long-chain alkanol sites on the nicotinic acetylcholine receptor and their allosteric interaction, *Biochemistry 40*, 11121−11130.
10. Arias, H. R., Trudell, J. R., Bayer, E. Z., Hester, B., McCardy, E. A., and Blanton, M. P. (2003) Noncompetitive antagonist binding sites in the *Torpedo* nicotinic acetylcholine receptor ion channel. Structure−activity relationship studies using adamantane derivatives, *Biochemistry 42*, 7358−7370.
11. Arias, H. R., McCardy, E. A., Bayer, E. Z., Gallagher, M. J., and Blanton, M. P. (2002) Allosterically linked noncompetitive antagonist binding sites in the resting nicotinic acetylcholine receptor ion channel, *Arch. Biochem. Biophys. 403*, 121−131.
12. Lurtz, M. M., and Pedersen, S. E. (1999) Aminotriarylmethane dyes are high-affinity noncompetitive antagonists of the nicotinic acetylcholine receptor, *Mol. Pharmacol. 55*, 159−167.
13. Gumilar, F., Arias, H. R., Spitzmaul, G., and Bouzat, C. (2003) Molecular mechanisms of inhibition of nicotinic acetylcholine receptors by tricyclic antidepressants, *Neuropharmacology 45*, 964−976.
14. Arias, H. R., Blanton, M. P., and Kem, W. R. (2004) Modulation of nicotinic acetylcholine receptors by anabaseine analogs. *Biophys. J. 86*, 545a (Abstr. 2824).
15. Pedersen, S. E., Dreyer, E. B., and Cohen, J. B. (1986) Location of ligand-binding sites on the nicotinic acetylcholine receptor α-subunit, *J. Biol. Chem. 261*, 13735−13743.
16. Marquardt, D. W. (1959) Solution of nonlinear chemical engineering models, *Chem. Eng. Prog. 55*, 65−70.
17. Moore, M. A., and McCarthy, M. P. (1995) Snake venom toxins, unlike smaller antagonists, appear to stabilize a resting state conformation of the nicotinic acetylcholine receptor, *Biochim. Biophys. Acta 1235*, 336−342.
18. Cheng, Y., and Prusoff, W. H. (1973) Relationship between the inhibition constant (K_i) and the concentration of inhibitor which causes 50% inhibition (IC_{50}) of an enzymatic reaction, *Biochem. Pharmacol. 22*, 3099−3108.
19. Schild, H. O. (1949) pA*x* and competitive drug antagonism, *Br. J. Pharmacol. 4*, 277−280.
20. Arias, H. R., McCardy, E. A., and Blanton, M. P. (2001) Characterization of the dizocilpine binding site on the nicotinic acetylcholine receptor, *Mol. Pharmacol. 59*, 1051−1060.
21. Aracava, Y., and Albuquerque, E. X. (1984) Meproadifen enhances activation and desensitization of the acetylcholine receptor-ionic channel complex (AChR): single channel studies, *FEBS Lett. 174*, 267−274.
22. Arias, H. R., Sankaram, M. B, Marsh, D., and Barrantes, F. J (1990) Effect of local anaesthetics on steroid-nicotinic acetylcholine receptor interactions in native membranes of *Torpedo marmorata* electric organ. *Biochim. Biophys. Acta 1027*, 287−294.
23. Bouzat, C., Bren, N., and Sine, S. M. (1994) Structural basis of the different gating kinetics of fetal and adult nicotinic acetylcholine receptors. *Neuron 13*, 1395−1402.
24. Hamill, O. P., Marty, A., Neher, E., Sakman, B., and Sigworth, F. J. (1981) Improved patch-clamp techniques for high-resolution current recording from cells and cell-free membrane patches. *Pfluegers Arch. 391*, 85−100.
25. Liu, Y., and Dilger, J. P. (1991) Opening rate of acetylcholine receptor channels. *Biophys. J. 60*, 424−432.
26. Spitzmaul, G., Dilger, J. P., and Bouzat, C. (2001) The noncompetitive inhibitor quinacrine modifies the desensitization kinetics of muscle acetylcholine receptors. *Mol. Pharmacol. 60*, 235−243.
27. Unwin, N. (2005) Refined structure of the nicotinic acetylcholine receptor at 4 Å resolution, *J. Mol. Biol. 346*, 967−989.
28. Oswald, R. E., Bamberger, M. J., and McLaughlin, J. T. (1984) Mechanism of phencyclidine binding to the acetylcholine receptor from *Torpedo* electroplaque, *Mol. Pharmacol. 25*, 360−368.
29. Arias, H. R (2001) Thermodynamics of Nicotinic Receptor Interactions, in *Drug-Receptor Thermodynamics*: *Introduction and Applications* (Raffa, R. B., Ed.) pp 293−358, John Wiley & Sons, New York.
30. Arias, H. R., McCardy, E. A., Gallagher, M. J., and Blanton, M. P. (2001b) Interaction of barbiturate analogs with the *Torpedo californica* nicotinic acetylcholine receptor ion channel, *Mol. Pharmacol. 60*, 497−506.
31. Mosckovitz, R., Haring, R., Gershoni, J. M., Kloog, Y., and Sokolovsky, M. (1987) Localization of azidophencyclidine-binding site on the nicotinic acetylcholine receptor α-subunit, *Biochem. Biophys. Res. Commun. 145*, 810−816.
32. Pratt, M. B., Pedersen, S. E., and Cohen, J. B. (2000) Identification of the sites of incorporation of [^{3}H]ethidium diazide within the *Torpedo* nicotinic acetylcholine receptor ion channel, *Biochemistry 39*, 11452−11462.
33. Eaton, M. J., Labarca, C., and Eteroviæ, V. A. (2000) M2 Mutations of the nicotinic acetylcholine receptor increase the potency of the noncompetitive inhibitor phencyclidine, *J. Neurosci. Res. 61*, 44−51.
34. Eteroviæ, V. A., Lu, R., Eakin, A. E., Rodriguez, A. D., and Ferchmin, P. A. (1999) Determinants of phencyclidine potency on the nicotinic acetylcholine receptors from muscle and electric organ, *Cell Mol. Neurobiol. 19*, 745−757.
35. Ho, K., and Flood, P. (2004) Single amino acid residue in the extracellular portion of transmembrane segment 2 in the nicotinic α7 acetylcholine receptor modulates sensitivity to ketamine, *Anesthesiology 100*, 657−662.
36. Gallagher, M. J., Chiara, D. C., and Cohen, J. B. (2001) Interactions between 3-(trifluoromethyl)-3-(m-[^{125}I]iodophenyl)-diazirine and tetracaine, phencyclidine, or histrionicotoxin in the *Torpedo* species nicotinic acetylcholine receptor ion channel, *Mol. Pharmacol. 59*, 1514−1522.
37. Middleton, R. E., Strnad, N. P., and Cohen, J. B. (1999) Photoaffinity labeling the *Torpedo* nicotinic acetylcholine receptor

with [^{3}H]tetracaine, a nondesensitizing noncompetitive antagonist, *Mol. Pharmacol. 56*, 290−299.
38. Gallagher, M. J., and Cohen, J. B. (1999) Identification of amino acids of the *Torpedo* nicotinic acetylcholine receptor contributing to the binding site for the noncompetitive antagonist [^{3}H]tetracaine, *Mol. Pharmacol. 56*, 300−307.
39. Dilger, J. P., Boguslavsky, R., Barann, M., Katz, T., and Vidal, A. M. (1997) Mechanism of barbiturate inhibition of acetylcholine receptor channels. *J. Gen. Physiol. 109*, 401−414.
40. Schlesinger, F., Krampfl, K., Haeseler, G., Dengler, R., and Bufler, J. (2004) Competitive and open channel block of recombinant nAChR channels by different antibiotics. *Neuromuscular Disord. 14*, 307−312.
41. Forman, S. A. (1999) A hydrophobic photolabel inhibit nicotinic acetylcholine receptors via open-channel block following a slow step. *Biochemistry 38*, 14559−14564.
42. Sine, S. M., and Taylor, P. (1982) Local anesthetics and histrionicotoxin are allosteric inhibitors of the acetylcholine receptor. Studies of clonal muscle cells, *J. Biol Chem. 257*, 8106−8114.
43. Ryan, S. E., Blanton, M. P., and Baenzinger, J. E. (2001) A conformational intermediate between the resting and desensitized states of the nicotinic acetylcholine receptor. *J. Biol. Chem. 276*, 4796−4803.

BI051752E